OCCASION

This publication has been made available to the public on the occasion of the 50th anniversary of the United Nations Industrial Development Organisation.

DISCLAIMER

FAIR USE POLICY

CONTACT

Please contact publications@unido.org for further information concerning UNIDO publications.

For more information about UNIDO, please visit us at www.unido.org

UNITED NATIONS INDUSTRIAL DEVELOPMENT ORGANIZATION
Vienna International Centre, P.O. Box 300, 1400 Vienna, Austria
Tel: (+43-1) 26026-0 · www.unido.org · unido@unido.org

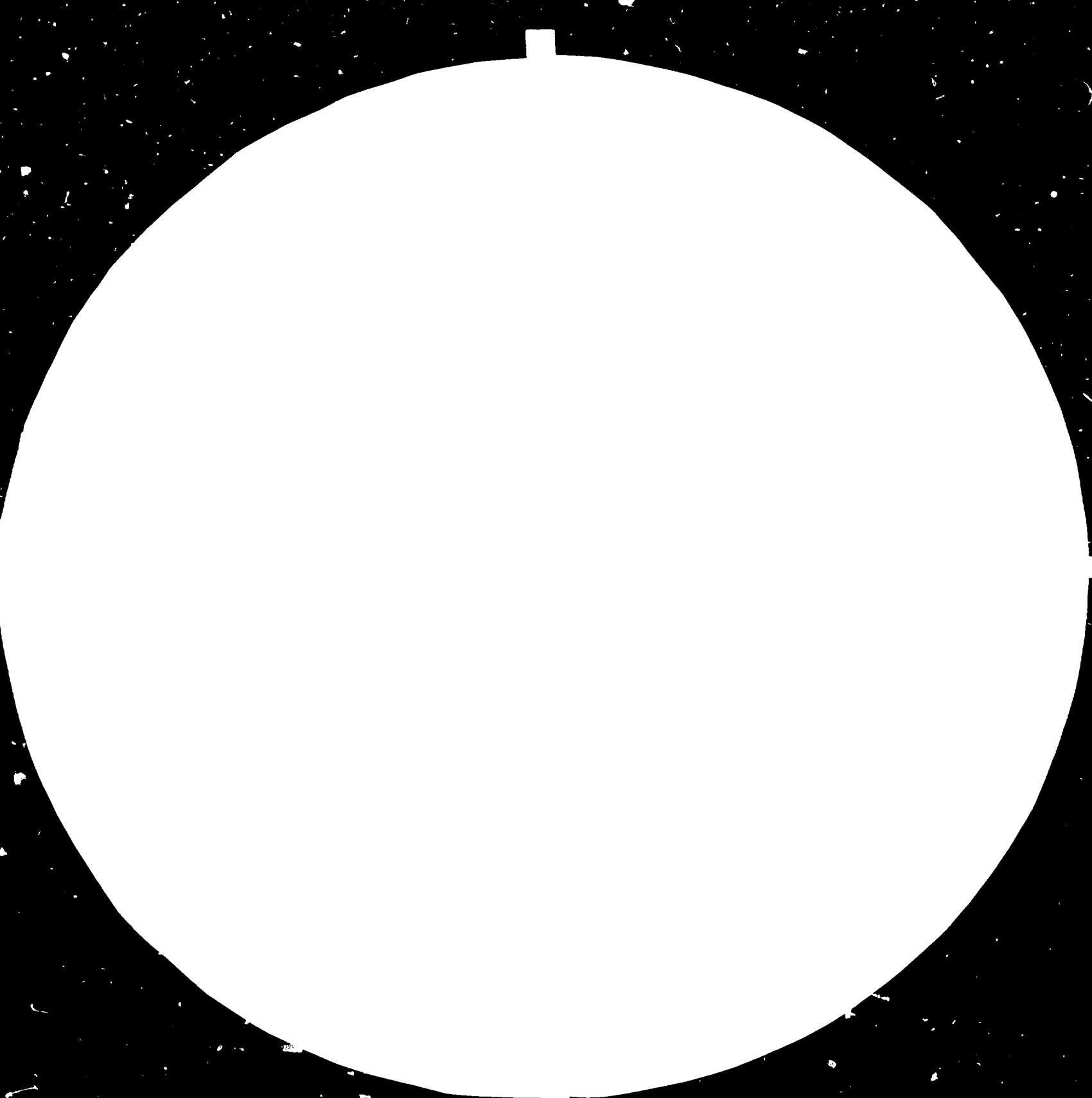

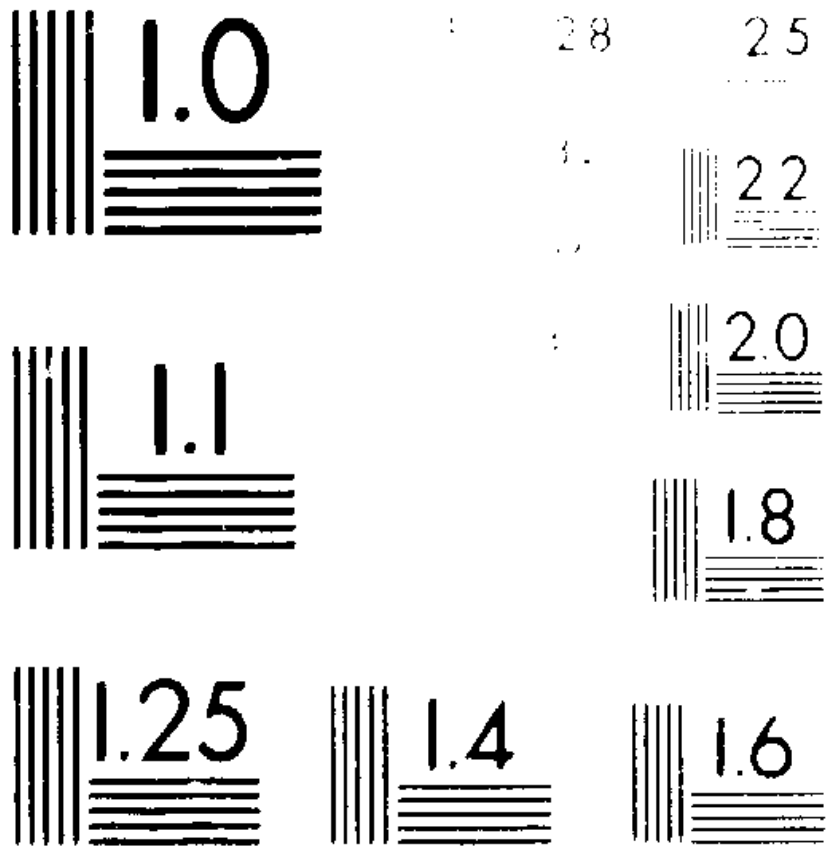
1.0
2.8
2.5
2.2
1.1
2.0
1.8
1.25
1.4
1.6

13936

RESTRICTED

June 1984

ENGLISH

BIOSCIENCE AND ENGINEERING

DP/IND/80/003

INDIA

Technical Report*

Mission 1-13 January 1984

Prepared for the Government of the Republic of India
by the United Nations Industrial Development Organization,
acting as executing agency for United Nations Development Programme

Based on the work of Liang-tseng Fan,
Consultant on Conversion of Glucose to Ethanol

United Nations Industrial Development Organization
Vienna

* This document has been reproduced without formal editing.

TABLE OF CONTENTS

1. TERMS OF REFERENCE

Duties

The consultant will in an advisory capacity assist the scientists from the National Chemical Laboratory in their studies on conversion of glucose to ethanol through an immobilized yeast cell process and will specifically advise on:

- production of ethanol from molasses with immobilized yeast packed bed reactor;
- strategies for scaling up programmes;
- reactor design, quality control of feed stream and waste disposal.

The consultant is expected to participate in the International Chemical Reaction Engineering Conference 9-11 January, 1984, Pune, organized by NCL. He will submit a brief report on his findings and recommendations.

2. SCHEDULE OF ACTIVITES

Activities and Actions

1. I arrived in the Pune airport on the early morning of 1 January, 1984. Dr. N. G. Karanth, who is heading the biochemical engineering group of National Chemical Laboratory (NCL) and is a key participant in the project, was at the airport to meet me.
2. Dr. Karanth escorted me to Hotel Amir. Immediately after check-in, I handed Dr. Karanth two packages containing copies of the research brochure and publications of my research group; many of the publications are related directly or indirectly to the project. Dr. Karanth discussed with me the program schedule (see Attachment 1).
3. On the second day of January, I met numerous project participants associated mainly with the Chemical Engineering Division of NCL, and discussed various matters, technical and otherwise, related to the project. Dr. Karanth guided me through the laboratory and pilot plant of the biochemical engineering group.
4. The third day of January was spent mainly visiting with the project participants associated with the Biochemistry Division; this group is headed by Dr. M. C. Scrinivasan. During discussion with him and his associates, I reaffirmed my willingness to accept one or more of them in my laboratory for the purpose of training them through cooperative research effort. Dr. Scrinivasan guided me through the major laboratories of his group and explained in some detail the activities conducted in these laboratories. Discussions were exchanged with many of the personnel of the laboratories on cellulose hydrolysis and related subjects.

5. During the third day of January, I also delivered a lecture to the researchers of NCL; it started at 11:30 AM and finished at 1:00 PM. In the lecture, I outlined the research activiteis of my group, much of which is closely related to the UNDP project at NCL.

6. Discussion on the research activities of my group presented in my lecture was held after lunch. The major focus of the discussion was on the pretreatment and hydrolysis of cellulose and fermentation of glucose (the product of hydrolysis). Technical and economic pros and cons of various procedures, methods and processes were debated intensively.

7. The fourth day and fifth day of January were spent participating in the 36-th annual session of the Indian Institute of Chemical Engineers held in Pune. I was accompanied by Dr. Karanth and some other members of the UNDP group. This meeting was also the first joint session with the Institution of Chemical Engineers (U.K.). Several papers were presented by members of the UNDP group of NCL. Whenever appropriate, I commented on their works during the 2-day session.

8. During the ninth day through the eleventh day of January, I participated in the International Chemical Reaction Engineering Conference organized by and held at NCL. I chaired a session in which Prof. Ramkrishna of Purdue University delivered a plenary lecture entitled CYBERNETIC MODELING OF MICROBIAL CELL POPULATION. This is a topic of vital importance to the development of a continuous fermentor or bioreactor for ethanol production. I also presented a paper at another session. Discussions were continued with numerous researchers of NCL on various topics related to my assigned consulting activities.

9. On the eleventh day of January, I conferred with a group of researchers headed by Dr. Mela Rao from Dr. Scrinivasen's laboratory on the cooperative work to be carried out between his group and mine. In fact, this work has been initiated and has been conducted mainly in my laboratory by Miss Seeta Ryali from Dr. Scrinivasen's group under UNDP sponsorship.

10. I departed from Pune on 12 January and returned to the U.S. on 15 January via Madras and Bombay. Two lectures were delivered in Madras, one at the Indian Institute of Technology, Madras and the other at the A.C. College of Engineering.

3. FINDINGS AND RECOMMENDATIONS

1. A systematic kinetic study has not been carried out on inhibition of P. funiculosum cellulase. It is urgent that such a study be carried out immediately. Glucose and cellobiose should be employed to induce inhibition. As stated previously, this effort is currently being conducted in my laboratory by Miss Seeta Ryali from NCL.

2. Pretreatment is a major process step contributing to the cost of enzymatic hydrolysis of cellulose. So far the UNDP group at NCL has paid relatively little attention to this step. An exhaustive study should be carried out on the effect of pretreatment on the rate of hydrolysis of various cellulosic materials by P. funiculosum. The recommended procedures are based on the facilities available in my laboratory. Description is given in Attachment 2. The expected benefit from such a study is also delineated in this attachment.

3. It appears that only a columnar (straight cylindrical) fluidized bed is used by the biochemical engineering group of NCL in continuous production of ethanol. Such a fluidized bed has numerous disadvantages for this application. This group should consider seriously the use of the tapered fluidized bed as a continuous bioreactor for production of alcohol by means of immobilized cells to reduce their elutriation. The advantages of the tapered fluidized bed over the columnar fluidized bed and the underlying hydrodynamics in the former are detailed in Attachment 3.

ATTACHMENT 1

Programme schedule of UNDP Consultant

Professor L.T. Fan

1 January 1984		Arrival Pune
2 January	9.30 - 10.00	Dr. R.A. Mashelkar, Head, C
	10.00 - 12.00	Dr. N.G. Karanth
	1.00 - 2.30	Lunch
	2.30 - 3.00	Dr. L.K. Doraiswamy, Directo NCL.
	3.00 - 3.30	Dr. B.D. Kulkarni
	3.30 - 4.00	Dr. V.S. Patwardhan
	4.00 - 4.30	Dr. R.V. Chaudhari
3 January	9.30 - 11.30	Dr. M.C. Srinivasan, Biochemistry Division
	11.30 - 1.00	Lecture
	1.00 - 2.30	Lunch
	2.30 - 4.30	Discussions with UNDP gr
4 January	9.15 - 4.00	IIChE 36th Annual Sessio at Tilak Smarak Mandir, Pu
5 January	9.00 - 6.00	-do-
9-11 January		ICREC
12 January		Departure

ATTACHMENT 2

PRETREATMENT OF CELLULOSIC MATERIAL

General Plan of Approach

Experiments will be designed to determine the effects of various pretreatment schemes on the rate and extent of enzymatic conversion.

First, the structural parameters of several types of untreated agricultural residues, including wheat straw and corn stover, will be determined. The structural parameters to be measured include crystallinity, specific surface area, lignin content, particle and pore-size distributions, and the appearance under scanning electron microscopy. Various treatment schemes will be considered. Enzymatic hydrolysis will be performed on the treated substrates, and the rate and extent of hydrolysis will be determined for each treated substrate. Acid hydrolysis will also be performed for comparison. The thermodynamic and economic feasibilities of enzymatic hydrolysis processes with several conbinations of pretreatment and substrate which are found to be promising will be examined.

Experimental Methods and Procedures

Cellulose. The substrates which will be used are agricultural cellulosic wastes, e.g., wheat straw and corn stover, as well as pure cellulose, e.g., sulfite bleached wood pulp, as a control.

Pretreatment. Pretreatment methods that will be used include ball-milling, roller-milling, Fitz-milling, caustic soda treatment, ethylene glycol treatment, and sodium sulfite treatment. The procedures are outlined below.

Ball-milling will be performed in a 5 liter jar mill charged to 50 volume percent with 1" porcelain or stainless steel balls. Roller-milling will be performed by recycling the wheat straw for extended periods of time. Fitz-milling will be carried out in a Model D, comminutor Fitz-mill (Fitz Patrick Company, Elmhurst, Illinois). Two different screen sizes will be used to achieve different extents of size reduction.

Treatment with 1% sodium hydroxide will be performed at room temperature or at autoclave conditions of 125°C and 2.2 atm. The treated substrate will be washed with water until the wash water is neutral. Treatment with 13.7% sodium sulfite solution will be carried out at room temperature or at autoclave conditions of 125°C and 2.2 atm. The substrate will be thoroughly washed as before. Treatment with ethylene glycol will be performed in presence of hydrochloric acid catalyst inside the autoclave at 125°C and 2.2 atm.

Parameter Measurement. The crystallinity of cellulose will be measured from x-ray diffraction data using the powder spectrometric technique employing parafocusing (Segal, et al., 1959). A crystallinity index (CrI) proposed by Segal, et al., (1959) is calculated with the intensities of diffraction at two different angles, 2θ:

$$CrI = \frac{I_{002} - I_{am}}{I_{002}} \times 100$$

where I_{002} is the intensity of diffraction of the 002 plane (2 = 22°) and I_{am} is the amorphous diffracted intensity (2 = 18°).

The specific surface areas of the cellulosic samples will be measured by applying the BET equation to nitrogen adsorption data collected from a Perkin-Elmer flow sorptometer. Pore size distributions will also be measured with this apparatus.

Lignin determinations will be performed in an analytical laboratory using the Van Soest fraction method (Goering and Van Soest).

Gel permeation chromatography (GPC) of cellulose for the measurement of the degree of polymerization will be carried out using high pressure liquid chromatography. [(Chang et al., 1973)].

A model Zf Coulter Counter employing hydrodynamic focusing will be used for particle size measurement.

Scanning electron and light microscopy will be employed to obtain additional insight into structural changes brought about by the pretreatments.

Hydrolysis. Hydrolysis of the pretreated or retreated cellulosics will be carried out at 5 wt. % concentration in a citric acid buffer and enzyme solution at 50°C and 250 r.p.m. The enzyme will be prepared from cultivations of the fungus Trichoderma reesei QM 9414. Reducing sugar production will be measured using the dinitrosalicylic acid (DNS) method (and HPLC).

Acid Hydrolysis. Acid hydrolysis of the cellulosic samples will be carried out in 10% and 80% by weight sulfuric acid at 120°C and 30°C, respectively.

Economic Feasibility Study. A series of economic feasibility studies will be analytically conducted by employing an exhaustive data base compiled in our preliminary work (Fan et al., 1977, 1980a, b; Beardmore et al., 1978; Beardmore, 1979) along with experimental results to be obtained in this proposa research. Various flow sheets will be developed to determine what combinations of pretreatment and/or retreatment schemes and operating conditions that will yield technically efficient and economically feasible enzymatic hydrolysis processes.

Thermodynamic Feasibility Study. A series of thermodynamic feasibility studies will be conducted by employing an exhaustive data base compiled in our previous works (Fan, et al., 1980a, b; 1981a, b) in conjunction with experimental results to be obtained in this proposed research. An analysis based on energy (Fan and Shieh, 1980; also see the appendix) will be applied. This will lead to an identification of energy efficient pretreatment schemes.

Assessment of Waste Treatment Schemes. Any pretreatment, particularly chemical, generates waste which can be an environmental pollutant if not properly treated or disposed. Waste treatment and disposal techniques for each pretreatment employed will be assessed for their technical and economic feasibility.

POTENTIAL CONTRIBUTION

Cellulose combined with extraneous material, such as lignin and hemicellulose, exists in nature in a crystalline structural form. The complexity and density of cellulosic material make it very resistant to attack by cellulolytic enzymes. Thus, its susceptibility to hydrolytic enzyme attack depends significantly on its structural features. The major structural features of cellulosic material that determine its susceptibility to enzymatic degradation include: (1) the degree of water swelling, (2) the crystallinity, (3) the molecular arrangement, (4) the content of associated material such as lignin, and (5) the capillary structure of cellulose fibers (Fan et al., 1977, 1980a, 1980b, 1981).

Cowling (1975) and Stone et al. (1969) have postulated that the most important structural feature that affects the enzymatic hydrolysis is the capillary structure of a cellulose fiber, because the susceptibility of cellulose to hydrolysis is determined largely by the accessibility of the cellulose surface to cellulolytic enzymes. Direct physical contact between the enzyme molecules and the substrate cellulose is a prerequisite to hydrolysis. According to Cowling (1975), any structural feature that limits the accessibility of cellulose to cellulase enzyme will diminish its susceptibil: to hydrolysis. The dimensions of the cellulose capillaries have been determ: by the solute exclusion technique (Aggebrandt and Samuelson, 1964; Van Dyke, 1972). Stone et al. (1969) used this technique to calculate the surface area within cellulose fibers swollen by phosphoric acid. The substrate was treated with a commercial cellulase enzyme preparation, and the initial rate of hydrolysis was compared with the accessibility of the substrate to molecu of various sizes. They reported a linear relationship between the initial

reaction rate and the surface area that was accessible to a molecule with a diameter of 40 Å. This diameter is equivalent to that of the cellulolytic enzyme. It appears, however, that little has been done to relate the surface area to the rate of hydrolysis for different kinds of natural cellulose substrates.

Another important structural parameter that affects enzymatic hydrolysis of cellulose is the degree of crystallinity of cellulose. Norkrans (1950) and Walseth (1952) showed that cellulolytic enzymes readily degrade the more accessible amorphous portion of regenerated cellulose but are less able to attack the less accessible crystalline portion. Consequently, a significant increase in crystallinity is observed during enzymatic hydrolysis of cellulose (Caulfield and Moore, 1974). As the cellulose becomes more crystalline, it becomes more resistant to further hydrolysis (Reese, et al., 1957; Nisizawa, 1973). The fraction of crystalline regions in the total cellulose can be expressed by an X-ray crystallinity index. An empirical method for determining the crystallinity of native cellulose using an X-ray diffractometer was studied by Segal et al. (1959). Baker et al. (1959) obtained an inverse relationship between the crystallinity index and digestibility of cellulose. However, Caulfield and Moore (1974) obtained somewhat different conclusions. Their X-ray measurements of the degree of crystallinity of ball-milled cellulose before and after partial hydrolysis indicate that ball-milling increases the susceptibility of both the amorphous component and the crystalline component of cellulose. They found that the enzyme digestibility of the crystalline component is enhanced to a greater extent by grinding than the amorphous component. They proposed that the overall increase in digestibility is apparently a result of decreased particle size and increased available surface area rather than a result of reduced crystallinity. They suggest coupling crystallinity investigation with

surface area measurements to effectively study the influence of each aspect of morphology.

Lignin is another important structural feature which limits the susceptibility of lignocellulosics. The combination of lignin with partially crystalline cellulose that exists in wood constitutes one of the nature's most biologically resistant system. Therefore, lignin removal is essential prior to enzymatic hydrolysis of lignocellulosics. The removal of the lignin from the lignocellulosics materials using various pretreatment methods leads to a marked increase in the hydrolysis rate (Han and Callihan, 1974; Kumakura and Kaetsu, 1979; Wilke, 1977). Lignin removal increases the availability of the carbohydrates to enzyme action through the disruption of the lignin carbohydrate linkage and swelling of the structure (Chahal et al., 1979; Kleinert, 1976).

Various chemical pretreatments methods have been used for delignification of lignocellulosics. For example, they include sodium hydroxide (Dunlap et al., 1976; Feist et al., 1970; Millet et al., 1976), sulfur dioxide (Millet et al., 1975), and sodium sulfide (Bellamy 1975, 1977).

Molecular weight distribution is an important parameter for understanding the mechanism of enzyme action. Enzymatic hydrolysis of cellulose is in reality a depolymerization reaction, which is promoted by various enzyme components. Several investigators (Nelson and Tripp, 1973; Battista et al., 1956; Chang et al., 1973; Nickerson and Habrle, 1947) observed a drastic drop in the degree of polymerization upon acid hydrolysis in the initial reaction period, whereas the degree of polymerization does not decrease substantially upon enzymatic hydrolysis (Walseth, 1952; Reese et al., 1957). Measurement of changes in the degree of polymerization will be useful in understanding the chemical mechanism of enzyme action, and the difference

between it and acid action.

In our earlier work we examined several important structural features affecting the enzymatic hydrolysis of Solka floc and wheat straw (Fan et al., 1977, 1980 a,b, 1981 a,b). We determined the relative effects of these structural features on the hydrolysis rate.

Ball-milling has been shown to be a highly effective pretreatment of cellulosic materials (Mandels et al., 1974). Our experiments show that after 96 hours of milling, a more than two fold increase in the rate of hydrolysis is obtained. The shearing and crushing effect of milling destroys the cellulose crystallinity and decreases its particle size.

Roller-milling has been shown to be an effective pretreatment of cellulosic materials (Tassinari and Macy, 1977). Our experiments have revealed a 3 fold increase in the rate of hydrolysis, after 30 minutes of milling. The shearing and crushing action of milling also destroys the cellulose crystallinity and decreases its particle size.

Fitz-milling results in a drastic size reduction in a short period of time. Our results, however, indicate a minor increase in the rate of hydrolysis. The cutting action of fitz-milling causes the size reduction.

Sodium hydroxide is well known as a chemical treatment to increase the digestibility of cellulose (Mandels et al., 1974; Millett et al., 1975). Various concentrations of NaOH have been employed, but Millet et al. (1975) have indicated that 5 to 6 grams of NaOH per gram of substrate gives maximum digestibility for several natural substrates. The mechanism of action involves swelling of the cellulose structure. Heating the cellulose with sodium hydroxide solution enhances this effect. Our previous work (Fan et al., 1980 a,b) showed a 50% increase in digestibility for pure cellulose fibers and a 250% increase for wheat straw with this technique.

Ethylene glycol has been shown to be a highly effective pretreatment for agricultural residues (Pannir Selvam and Ghose, 1980). Our results also indicate a 9 fold increase in the rate of hydrolysis of wheat straw after ethylene glycol pretreatment. The solvent action of ethylene glycol leads to a high delignification. This pretreatment can be promising provided that an efficient process is developed for recovering and recycling the ethylene glycol

Sodium sulfite has been traditionally used for pulping of lignocellulosics, e.g., wheat straw (Casey, 1960). Our results indicate a dramatic increase in the rate of hydrolysis after sulfite pretreatment. Chemical action of sulfite causes the delignification and structural swelling of substrate.

It can be stated that different treatment methods have different effects on lignocellulosic structure and increase the susceptibility of cellulose to enzyme action in different ways. This suggests that it is definitely feasible to develop an efficient enzymatic hydrolysis process or processes which combine more than one pretreatment or pretreatments with retreatments.

A study of the detailed mechanism of pretreatment of a lignocellulosic residue prior to its enzymatic hydrolysis, by examining the structural modification and its relationship to the rate of hydrolysis, will facilitate the optimal and rational selection of a pretreatment method. The extension of such a study to a variety of lignocellulosics will assist in making a choice of the most effective combination of the substrate and pretreatment method. The comparison of enzymatic versus acid hydrolyses will facilitate understanding the mechanisms of acid and enzymatic hydrolyses as they are affected by different pretreatment methods. The economic and thermodynamic analyses of different combinations of a substrate and a pretreatment method will be

useful for evaluating the feasibilities of their commercialization. Pre-treatments, especially chemical, generate waste which can cause environmental pollution, and hence, for an operating plant, treatment of such waste will be necessary prior to disposal.

REFERENCES

Aggebrandt, L. G. and O. J. Samuelson, J. Appl. Polymer Sci., 8, 2801 (1964).

Baker, T. I. et al., J. Animal Sci., 18, 655 (1959).

Battista, O. A. et al., Ind. Eng. Chem., 48, 333 (1956).

Bellamy, W. D., in Single Cell Protein II, S. R. Tannebaum and D. I. C. Wang, Eds. (The MIT Press, Cambridge, Mass., 1975), p. 263.

Bellamy, W. D., Develop. Ind. Microbiol., 18, 249 (1977).

Beardmore, D. H., Y. H. Lee, and L. T. Fan, in Proceed. Eighth Ann. Biochem. Eng. Symp., C. E. Dunlap, Ed. (Univ. of Missouri, Columbia, Missouri, 1978), p. 38.

Beardmore, D. H., Y. H. Lee, and L. T. Fan, in Proceed. Ninth Ann. Biochem. Eng. Symp., L. T. Fan and L. E. Erickson, Eds. (Kansas State Univ., Manhattan, Kansas, 1979), p. 66.

Casey, J. P., in Pulp and Paper Vol. 1, 2nd Edit., (Interscience, N.Y., 1960, p. 100.

Caulfield, D. F. and W. E. Moore, Wood Science, 6, 375 (1974).

Chahal, D. S., M. Moo-Young, and G. S. Dhillon, Can. J. Microbiol., 25, 793 (1979).

Chang, M., T. C. Pound, and John R. S. T. Manley, J. Polymer Sci., A-2, 11, 399 (1973).

Cowling, E. B., Biotechnol. Bioeng. Symp. No. 5, 163 (1975).

Dunlap, C. E., J. Thomson, and L. C. Chiang, AIChE Symp. Ser. No. 158, 58 (1976).

Fan, L. T., Y. H. Lee, and L. S. Fan, in Proceed. Seventh Ann. Biochem. Eng. Symp., P. Reilly, Ed. (Engineering Research Institute, Iowa State University, Ames, Iowa, 1977).

Fan, L. T., Y. H. Lee, and D. H. Beardmore, Biotechnol. Bioeng., 22, 177 (1980 a).

Fan, L. T., Y. H. Lee, and D. H. Beardmore, in Adv. Biochem. Eng. Vol. 14, A Fiechter, Ed. (Springer-Verlag, Berlin, 1980 b), p. 101

Fan, L. T., and J. H. Shieh, Energy, 5, 955 (1980).

Fan, L. T., Y. H. Lee, and D. H. Beardmore, Biotechnol. Bioeng., 23, 419 (1981 a).

Fan, L. T., M. M. Gharpuray, and Y. H. Lee, Biotechnol. Bioeng. Symp. No. 11, 29 (1981).

Feist, W. C., A. J. Baker, and H. Rarkow, J. Anim. Sci., 30, 832 (1970).

Goering, H. K. and P. J. Van Soest, Forage Fiber Analyses, Agriculture Handbook (U.S. Dept. of Agriculture, Wash. D. C.)

Han, Y. W. and C. D. Callihan, Appl. Microbiol., 27, 1959 (1974).

Kleinert, T. N., Tappi, 59, 122 (1976).

Kumakura, M. and I. Kaetsu, Biotechnol. Bioeng., 20, 1309 (1979).

Mandels, M., L. Hontz, and J. Nystrom, Biotechnol. Bioeng., 16, 1471 (1974).

Millett, M. A. et al., J. Anim. Sci., 31, 1781 (1970).

Millett, M. A., A. J. Baker, and L. D. Satter, in Biotechnol. Bioeng. Symp. No. 5, C. R. Wilke, Ed. (Wiley Interscience, 1975), p. 193.

Millett, M. A., A. J. Baker, and L. D. Satter, Biotechnol. Bioeng. Symp. No. 6, 125 (1976).

Moore, W. E., M. J. Effland, and M. A. Millett, J. Agr. Food Chem., 20, 1173 (1972).

Nickerson, R. F. and J. A. Habrle, Ind. Eng. Chem., 39, 1507 (1947).

Nelson, M. A. and V. M. Tripp, J. Polymer Sci., 10, 577 (1953).

Nisizawa, K., J. Ferment. Technol., 51, 267 (1973).

Norkrans, B., Physical Plant, 3, 75 (1950).

Pannir Selvam, P. V. and T. K. Ghose, Presented at the Second International Symposium on Bioconversion and Biochemical Engineering, IIT, Delhi, March 3-6, 1980.

Reese, E. T., L. Segal, and V. M. Tripp, Text. Res. J., 27, 626 (1957).

Sasaki, T., S. Nakagawa, and K. Kainuma, Presented at the American Association of Cereal Chemists Annual Meeting, San Francisco, 1977.

Segal, L. et al., Text. Res. J., 29, 786 (1959).

Stone, J. E. et al., in Cellulases and their Applications, G. J. Hajny and E. T. Reese, Eds. (ACS, Washington, D.C., 1969), p. 219.

Tassinari, T. and C. Macy, Biotechnol. Bioeng., 19, 1321 (1977).

Tsao, G. T., US/ROC Joint Seminar; Fermentation Engineering (Philadelphia, Pa., 1978).

Van Dyke, B. H., Jr., "Enzymatic Hydrolysis of Cellulose-A Kinetic Study," Ph.D. dissertation, M.I.T., Cambridge, Mass., 1972.

Walseth, C. S., Tappi, 35, 233 (1952).

Wilke, C. R., Pilot Plant Studies on the Bioconversion of Cellulose and Production of Ethanol, Lawrence Berkeley Lab. Report No. LBL 6860, Univ. of Calif., Berkeley, Ca., June 1977.

ATTACHMENT 3

TAPERED FLUIDIZED BEDS

INTRODUCTION

Straight cylindrical or columnar fluidized beds have been employed extensively in the process industries. Recently, the use of tapered fluidized beds is beginning to receive much attention for biochemical reaction and biological treatment of waste water (see, e.g., Scott and Hancher, 1976; Pitt et al., 1981). Tapered fluidized beds have also been used successfully in chemical reactions, crystallization, and in other areas (see, e.g., Levey et al., 1960, Ishii, 1973; Golubkovich, 1975; Dighe et al., 1981).

Features of the tapered fluidized bed, especially its advantages over the columnar fluidized bed, are discussed below:

1. Usually the size distribution of a particle system which can be employed in a columnar fluidized bed need be narrow. If the particle size distribution is too broad, small particles may be entrained and large particles may be defluidized, settling on the distributor. The cross-sectional area of the tapered fluidized bed is enlarged along the bed height from the bottom to the top. Therefore, the velocity of the fluidizing medium is relatively high at the bottom, ensuring fluidization of the large particles, and it is relatively low at the top, preventing entrainment of the small particles. Therefore, we can operate the tapered fluidized bed with particles whose size distribution is wide. This feature is specially important for an operation in which the particle size changes (coal combustion, crystallization, microbial growth, etc.).

2. For an intensely exothermic reaction in the columnar fluidized bed the major fraction of heat is released near the distributor, creating a high temperature zone and possibly destroying the distributor and sintering the particles. However, in the tapered fluidized bed, the

velocity of the fluidizing medium at the bottom of the bed is fairly high. This gives rise to a low particle concentration, thus resulting in a low reaction rate and reduced rate of heat release. Therefore, the generation of a high temperature zone near the distributor can be prevented.

3. The velocity of the fluidizing medium at the bottom of the tapered fluidized bed can be greater than the terminal particle velocity. In this case the tapered fluidized bed can be operated without a distributor (Golubkovich, 1975).

4. For a deep gas-solids columnar fluidized bed, the pressure difference between the bottom and the top is large, and thus, the gas tends to expand as it rises through the bed, rendering the upward gas velocity to increase continuously and reaches the maximum at the top. This will tend to agitate the top of the bed violently; this promotes elutriation of the particles from the bed surface and instability (pressure fluctuations) in the bed. In contrast, the cross-sectional area of the tapered fluidized bed increases upward; this enables it to accommodate the increase in the gas volume, rendering it possible to operate smoothly with the deep bed (Ridgway, 1965).

Because of these advantages, the use of tapered fluidized beds is rapidly increasing; however, much is unknown concerning characteristics of the tapered fluidized bed. Hydrodynamic features of the tapered fluidized bed are very different from those of the columnar fluidized bed, as can be seen in Fig. 1 where typical pressure drop-velocity relations of the tapered bed (curve 1) and that of the columnar bed (curve 2) are shown. The superficial velocity of the fluidizing medium in the tapered bed indicated in the figure is based on the bottom cross-sectional

area. The static bed heights in the two beds are identical. This figure shows that the critical fluidizing velocity in terms of the superficial velocity at the bottom of the bed, u_c, at which the particles on the bottom of the tapered bed begin to fluidize, is greater than the minimum fluidizing velocity, u_{mf}. The maximum pressure drop, $(-\Delta P_{max})$, which is created at u_c in the tapered bed, is greater than the maximum pressure drop, $(-\Delta P_{mf})$, in a columnar bed. Therefore, the known hydrodynamic relations for the columnar bed cannot be directly applied to the tapered bed.

The objectives of this work were to propose a mechanistic model for the condition of incipient fluidization in the tapered bed, to derive equations for predicting the critical fluidizing velocity, u_c, and the maximum pressure drop, $(-\Delta P_{max})$, and to verify these equations experimentally.

THEORETICAL

Different views exist concerning the incipient fluidization condition of a tapered fluidized bed. Gelperin et al. (1960) have proposed that particles would fluidize when the superficial velocity of the fluidizing medium at the upper surface of the tapered fluidized bed reaches the minimum fluidizing velocity, u_{mf}. However, the calculated critical fluidizing velocity in terms of the superficial velocity at the bottom of the bed, u_c, and the calculated maximum pressure drop, $(-\Delta P_{max})$, based on their model are appreciably greater than the experimental data. Nishi (1979) has proposed that when the pressure drop in the tapered bed is equal to the effective weight of the particles on the unit bottom cross-sectional area, i.e., at point B on Fig. 1, the particles would begin to fluidize. However, the observations made in our preliminary experiments have shown that the particles remain in a static state at point B, and that the critical fluidizing velocity, u_c, is higher than the calculated velocity by Nishi's equation, u', at point B.

In our preliminary experimental study, we have observed that when the fluid velocity increases, the pressure drop through the tapered bed also increases. At a certain velocity, the pressure drop through the bed reaches the maximum and the total particles in the bed are lifted upward by the fluid. At this moment, the particles at the bottom of the bed begin to fluidize; thereafter, the condition of fluidization will extend from the bottom to the top, and the pressure drop will decline fairly sharply, as depicted in Fig. 1. This experimental observation motivates us to postulate that fluidization is initiated when the force exerted by the fluidizing medium flowing through the bed is equal to the total effective weight of the material in the bed under the assumption that friction is negligible between the particles and bed walls. For simplicity, we further assume that the lateral velocity of the fluid is sufficiently small to be neglected and that the vertical velocity of the fluid is uniformly distributed on the cross-sectional area. The pressure drop through a packed bed with a differential height of dh is equal to (Ergun, 1952)

$$-dP = (Au + Bu^2)dh \tag{1}$$

where

$$A = 150 \frac{(1 - \varepsilon_0)^2}{\varepsilon_0^3} \frac{\mu}{(\phi_s d_p)^2}$$

$$B = 1.75 \frac{1 - \varepsilon_0}{\varepsilon_0^3} \frac{\rho_f}{\phi_s d_p}$$

The overall pressure drop across the entire bed height, H, is obtained by integrating equation (1), i.e.,

$$(-\Delta P) = \int_{P_{h_0}}^{P_{H+h_0}} (-dP) = \int_{h_0}^{H+h_0} (Au + Bu^2)\,dh \tag{2}$$

For a two-dimensional tapered bed with a thickness of w_0 and an apex angle of θ, we have (see Fig. 2)

$$u = u_\theta \frac{\ell_0}{\ell} = u_0 \frac{h_0}{h} \tag{3}$$

and

$$\ell_1 = \ell_0 + 2H\tan\frac{\theta}{2} \tag{4}$$

Therefore (see APPENDIX A),

$$(-\Delta P) = Au_0 \frac{H\ell_0}{\ell_1 - \ell_0} \ln\frac{\ell_1}{\ell_0} + Bu_0^2 \frac{H\ell_0}{\ell_1} \tag{5a}$$

or

$$(-\Delta P) = Au_0 \frac{\ell_0}{2\tan\frac{\theta}{2}} \ln\frac{\ell_0+2H\tan\frac{\theta}{2}}{\ell_0} + Bu_0^2 \frac{H\ell_0}{\ell_0+2H\tan\frac{\theta}{2}} \tag{5b}$$

Equations (5a) or (5b) can be rewritten in dimensionless form, respectively, as

$$Eu = 150 \frac{(1-\varepsilon_\theta)^2}{\phi_s^2\varepsilon_0^3} \frac{1}{Re}\frac{H}{d_p} \frac{\ell_0}{\ell_1 - \ell_0} \ln\frac{\ell_1}{\ell_0} + 1.75 \frac{1-\varepsilon_0}{\phi_s\varepsilon_0^3} \frac{H}{d_p}\frac{\ell_0}{\ell_1} \tag{6a}$$

or

$$Eu = 150 \frac{(1-\varepsilon_0)^2}{\phi_s^2\varepsilon_0^3} \cdot \frac{1}{Re}\frac{H}{d_p} \frac{\ell_0}{2H\tan\frac{\theta}{2}} \ln\frac{\ell_0+2H\tan\frac{\theta}{2}}{\ell_0} + 1.75 \frac{(1-\varepsilon_0)}{\phi_s\varepsilon_0^3} \frac{H}{d_p} \cdot \frac{\ell_0}{\ell_0 + 2H\tan\frac{\theta}{2}} \tag{6b}$$

The cross-sectional area of a tapered fluidized bed increases continuously from the bottom to the top; therefore, the force exerted by the fluidizing fluid on the particles is not directly proportional to the pressure drop. This force in a differential bed height of dh is equal to the product of the pressure drop through it, (-dP), and the cross-sectional area of the bed ℓw_0:

$$dF = \ell w_0(-dP) = \ell w_0(Au + Bu^2)dh \tag{7}$$

Thus, the overall force exerted by the fluidizing fluid on the particles in the entire bed with a height of H is (see APPENDIX B)

$$F = \int_0^F dF = \int_{h_0}^{H+h_0} \ell w_0(Au + Bu^2)dh \tag{8}$$

or

$$F = Au_0 w_0 \ell_0 H + Bu_0^2 \frac{w_0 \ell_0^2 H}{\ell_1 - \ell_0} \ln \frac{\ell_1}{\ell_0} \tag{9}$$

The overall effective weight of the particles in the bed is (see APPENDIX C)

$$G = \int_{h_0}^{H+h_0} g(1 - \varepsilon_0)(\rho_s - \rho_f)\ell w_0 dh$$

$$= \frac{g}{2}(1 - \varepsilon_0)(\rho_s - \rho_f)w_0 H(\ell_1 + \ell_0) \tag{10}$$

According to the proposed model, the particles on the bottom begin to fluidize when

$$F = G$$

Therefore, the critical fluidizing velocity, u_c, can be calculated by equating equations (9) and (10). This gives

$$\left(B \frac{w_0 \ell_0^2 H}{\ell_1 - \ell_0} \ln \frac{\ell_1}{\ell_0}\right) u_c^2 + (A\, w_0 \ell_0 H) u_c - \frac{1}{2}(1 - \varepsilon_0)(\rho_s - \rho_f) w_0 H (\ell_1 + \ell_0) g = 0 \qquad (11)$$

which, in turn, gives

$$u_c = \frac{-B' + \sqrt{B'^2 + 4A'C'}}{2A'} \qquad (12)$$

where

$$A' = B \frac{w_0 \ell_0^2 H}{\ell_1 - \ell_0} \ln \frac{\ell_1}{\ell_0} = B \frac{w_0 \ell_0^2}{2H\tan\frac{\theta}{2}} \ln \frac{\ell_0 + 2H\tan\frac{\theta}{2}}{\ell_0}$$

$$B' = A w_0 \ell_0 H$$

$$C' = \frac{1}{2}(1 - \varepsilon_0)(\rho_s - \rho_f) w_0 H (\ell_1 + \ell_0) g$$

$$= (1 - \varepsilon_0)(\rho_s - \rho_f) w_0 H (\ell_0 + H\tan\frac{\theta}{2}) g$$

The dimensionless form of equation (11) can be expressed as

$$1.75 \frac{1}{\phi_s \varepsilon_0^3} \frac{2\ell_0^2 \ln \frac{\ell_1}{\ell_0}}{\ell_1^2 - \ell_0^2} Re_c^2 + 150 \frac{1 - \varepsilon_0}{\phi_s^2 \varepsilon_0^3} \frac{2\ell_0}{\ell_1 + \ell_0} Re_c - Ar = 0 \qquad (13a)$$

or

$$1.75 \frac{1}{\phi_s \varepsilon_0^3} \frac{\ell_0^2}{2\tan\frac{\theta}{2}} \frac{\ln \frac{\ell_0 + 2H\tan\frac{\theta}{2}}{\ell_0}}{H(\ell_0 + H\tan\frac{\theta}{2})} Re_c^2 + 150 \frac{1 - \varepsilon_0}{\phi_s^2 \varepsilon_0^3} \frac{\ell_0}{\ell_0 + H\tan\frac{\theta}{2}} Re_c - Ar = 0 \qquad (13b)$$

Replacing u_0 in equation (5a) with u_c, the maximum pressure drop through the tapered bed $(-\Delta P_{max})$, is calculated as follows:

$$(-\Delta P_{max}) = Au_c \frac{H\ell_0}{\ell_1-\ell_0} \ln \frac{\ell_1}{\ell_0} + Bu_c^2 \frac{H\ell_0}{\ell_1} \tag{14a}$$

Equivalently, replacing u_0 in equation (5b) with u_c, we obtain

$$(-\Delta P_{max}) = Au_c \frac{\ell_0}{2\tan\frac{\Theta}{2}} \ln \frac{\ell_0 + 2H\tan\frac{\Theta}{2}}{\ell_0} + Bu_c^2 \frac{H\ell_0}{\ell_0 + 2H\tan\frac{\Theta}{2}} \tag{14b}$$

The dimensionless forms of these equations are, respectively,

$$Eu_c = 150 \frac{(1-\varepsilon_0)^2}{\phi_s^2\varepsilon_0^3} \frac{1}{Re_c} \frac{H}{d_p} \frac{\ell_0}{\ell_1-\ell_0} \ln \frac{\ell_1}{\ell_0} + 1.75 \frac{1-\varepsilon_0}{\phi_s\varepsilon_0^3} \frac{H}{d_p} \frac{\ell_0}{\ell_1} \tag{15a}$$

and

$$Eu_c = 150 \frac{(1-\varepsilon_0)^2}{\phi_s^2\varepsilon_0^3} \frac{1}{Re_c} \frac{1}{d_p} \frac{\ell_0}{2\tan\frac{\Theta}{2}} \ln \frac{\ell_0 + 2H\tan\frac{\Theta}{2}}{\ell_0} + 1.75 \frac{1-\varepsilon_0}{\phi_s\varepsilon_0^3} \frac{1}{d_p} \frac{H\ell_0}{\ell_0 + 2H\tan\frac{\Theta}{2}} \tag{15b}$$

EXPERIMENTAL

Facilities

A schematic of the experimental facilities is shown in Fig.3. The dimensions of the two-dimensional tapered beds employed are listed in Table 1. Notice that the apex angles of the two tapered beds were 20° and 30°.

All vessels were made of transparent acrylic resin so that the solids behavior could be observed. The distributor was a stainless steel screen of 48 mesh.

Materials

Silica gel and sand particles were fluidized. Characteristics of these particles are listed in Table 2. Water at room-temperature (approximately 20°C) was used as the fluidizing medium. The flow rate was measured by a rotameter, and the pressure drop was measured by a piezometer.

Procedure

A known weight of particles was poured into the bed, and then the particles were fluidized fully by water at a certain velocity. The loading of particles for each experiment ranged from 1 kg to 3.9 kg. When a stable state of fluidization was established, the values of the velocity and pressure drop were recorded as the velocity was gradually reduced to zero. When the velocity reached zero, the velocity was gradually increased, and the values of the velocity and pressure drop were again recorded. From these data the pressure drop-velocity curve was constructed. The critical fluidizing velocity, u_c, and the maximum pressure drop, $(-\Delta P_{max})$, were determined from the curve. The procedure described above gave a reproducible bed porosity even though the packed bed pressure drop is very sensitive to the bed porosity, and different degrees of packing of the particles produce different bed porosities.

RESULTS AND DISCUSSION

The experimental results have shown that the pressure drop-velocity diagram of the tapered fluidized bed indeed has the shape of curve 1 in Fig. 1; in the increasing fluid velocity cycle, the pressure drop reaches a maximum value and then decreases sharply, approaching an essentially constant value. In the decreasing fluid velocity cycle, however, the pressure drop decreases continuously and the peak is not recovered. This is similar to the pressure drop-velocity diagram of the columnar fluidized

bed. The difference between the diagram of the tapered bed and that of the columnar bed is that the peak in the former is much sharper than that of the latter.

A comparison of equation (5a) or (5b) with the experimentally measured pressure drop through the tapered packed bed shows that they are in good agreement (Fig. 4). Therefore, the assumptions that the lateral velocity of the fluid is negligible and the vertical velocity of the fluid is uniformly distributed seem to be reasonable. Figure 5 compares the critical fluidizing velocity, u_c, calculated by equation (12) with the experimental data, and Fig. 6 compares the maximum pressure drop, $(-\Delta P_{max})$, calculated by equation (14a) or (14b) with the experimental data. It is evident from these figures that the agreement between the calculated values and experimental data is satisfactory, indicating the proposed model is valid and the derived equations are of practical use.

When the apex angle becomes negligibly small, i.e., $\theta \to 0$, we have

$$\lim_{\theta \to 0} \frac{\ell_0^2 \cdot \ln \dfrac{\ell_0 + 2H\tan\frac{\theta}{2}}{\ell_0}}{H \cdot 2\tan\frac{\theta}{2} \cdot (\ell_0 + H\tan\frac{\theta}{2})} = 1$$

and

$$\lim_{\theta \to 0} \frac{\ell_0}{\ell_0 + H\tan\frac{\theta}{2}} = 1$$

Thus, equation (13b) reduces to

$$1.75 \frac{1}{\phi_s \varepsilon_0^3} Re^2 + 150 \frac{(1 - \varepsilon_0)}{\phi_s^2 \varepsilon_0^3} Re - Ar = 0 \qquad (16)$$

which is the well-known equation for predicting the minimum fluidizing velocity, u_{mf}, of the columnar fluidized bed (Kunii and Levenspiel, 1969). Furthermore, when $\theta \to 0$, or $\ell_1 \to \ell_0$, equation (14a) or (14b) reduces to

$$(-\Delta P_{max}) = Au_c H + Bu_c^2 H \tag{17}$$

and equation (11) reduces to

$$Bu_c^2 H + Au_c H - (1 - \varepsilon_0)(\rho_s - \rho_f)Hg = 0 \tag{18}$$

or

$$\begin{aligned}(-\Delta P_{max}) &= (1 - \varepsilon_0)(\rho_s - \rho_f)Hg \\ &= \frac{G}{w_0 \ell_0} \\ &= (-\Delta P_{mf})\end{aligned} \tag{19}$$

This is also a well-known result that relates the pressure drop at the minimum fluidizing velocity in the columnar bed, $(-\Delta P_{mf})$, to the effective weight of particles per unit cross-sectional area of the bed. These developments indicate that the proposed model is internally self-consistent.

In applying the proposed model to a gas-solids system, a further simplification can be made by letting $(\rho_s - \rho_f) = \rho_s$ because $\rho_s >> \rho_f$. Since such a system is usually non-particulate, some empirical modifications probably need be made on the model equations.

CONCLUSIONS

1. The hydrodynamic features of the tapered fluidized bed is very different from that of the columnar fluidized bed, and therefore, the known relations for the columnar bed cannot be used in calculating those for the tapered bed.

2. A model has been proposed for the condition of incipient fluidization in the tapered fluidized bed. Equations have been derived from the model for predicting the critical fluidizing velocity, u_c, and the maximum pressure drop, $(-\Delta P_{max})$. The experimental data obtained in two-dimensional, liquid-fluidized tapered beds indicate that the proposed model is valid and the derived equations are of practical use.

APPENDIX A. DERIVATIONS OF EQUATION (5a) AND EQUATION (5b) FROM EQUATION (2)

Equation (2) in the text is

$$(-\Delta P) = \int_{h_0}^{H+h_0} (Au + Bu^2)dh \qquad (A-1)$$

Since

$$u = u_0 \frac{\ell_0}{\ell} = u_0 \frac{h_0}{h}, \qquad (A-2)$$

we have

$$(-\Delta P) = \int_{h_0}^{H+h_0} (Au_0 \frac{h_0}{h} + Bu_0^2 \frac{h_0^2}{h^2})dh$$

$$= Au_0h_0 \ln \frac{H + h_0}{h_0} + Bu_0^2 \frac{Hh_0}{(H + h_0)} \qquad (A-3)$$

Furthermore, because

$$\frac{H + h_0}{h_0} = \frac{\ell_1}{\ell_0} = \frac{\ell_0 + 2H\tan \frac{\theta}{2}}{\ell_0}, \qquad (A-4)$$

we obtain

$$(-\Delta P) = Au_0 \frac{H\ell_0}{\ell_1 - \ell_0} \ln \frac{\ell_1}{\ell_0} + Bu_0^2 \frac{H\ell_0}{\ell_1} \qquad (A-5)$$

or

$$(-\Delta P) = Au_0 \frac{\ell_0}{2\tan \frac{\theta}{2}} \ln \frac{\ell_0 + 2H\tan \frac{\theta}{2}}{\ell_0}$$

$$+ Bu_0^2 \frac{H\ell_0}{\ell_0 + 2H\tan \frac{\theta}{2}} \qquad (A-6)$$

Equation (A-5) or (A-6) is the same as equation (5a) or (5b), respectively, in the text.

APPENDIX B. DERIVATION OF EQUATION (9)

From equation (A-2), we have

$$\ell = \frac{\ell_0}{h_0} h \text{ and } u = u_o \frac{\ell_0}{h} \tag{B-1}$$

Substituting these expressions into equation (8) leads to

$$F = \int_{h_0}^{H+h_0} [Aw_0u_0\ell_0 + Bw_0u_0^2\ell_0h_0 \frac{1}{h}] dh$$

$$= Aw_0u_0\ell_0 \, h \Big|_{h_0}^{H+h_0} + Bw_0u_0^2\ell_0h_0 \ell nh \Big|_{h_0}^{H+h_0}$$

$$= Aw_0u_0\ell_0H + Bw_0u_0^2\ell_0h_0 \ell n \frac{H+h_0}{h_0} \tag{B-2}$$

Since

$$\frac{H+h_0}{h_0} = \frac{\ell_1}{\ell_0} \tag{B-3}$$

or

$$h_0 = \frac{H\ell_0}{\ell_1-\ell_0} , \tag{B-4}$$

substituting these two equations into equation (B-1) yields

$$F = Aw_0u_0\ell_0H + Bw_0u_0^2 \frac{H\ell_0^2}{\ell_1-\ell_0} \ell n \frac{\ell_1}{\ell_0} \tag{B-5}$$

This is equation (9) in the text.

APPENDIX C. DERIVIATION OF EQUATION (10)

From equation (A-2), we have

$$\ell = \frac{\ell_0}{h_0} h \tag{C-1}$$

Substituting this equation into equation (10) gives

$$G = \int_{h_o}^{H+h_0} g(1-\varepsilon_0)(\rho_s-\rho_f)\ w_0 \frac{\ell_0}{h_0} h\ dh$$

$$= g(1-\varepsilon_0)(\rho_s-\rho_f)\ w_0 \frac{\ell_0}{h_0} \frac{h^2}{2}\Bigg|_{h_0}^{H+h_0}$$

$$= g(1-\varepsilon_0)(\rho_s-\rho_f)\ w_0 \frac{\ell_0}{h_0} \left(\frac{H^2+2Hh_0}{2}\right)$$

$$= \frac{1}{2} g(1-\varepsilon_0)(\rho_s-\rho_f)\ w_0 \frac{H\ell_0}{h_0} (H+2h_0) \tag{C-2}$$

From equation (B-3), we have

$$h_0 = \frac{H\ell_0}{\ell_1-\ell_0} \tag{C-3}$$

Substituting this equation into equation (C-2) yields

$$G = \frac{1}{2} g(1-\varepsilon_0)(\rho_s-\rho_f)\ w_0\ (\ell_1-\ell_0)\left(H+\frac{2H\ell_0}{\ell_1-\ell_0}\right)$$

or

$$G = \frac{g}{2}(1-\varepsilon_0)(\rho_s-\rho_f)\ w_0\ H\ (\ell_1+\ell_0) \tag{C-4}$$

This is the final expression of equation (10) in the text.

NOTATION

d_p = particle diameter [m]

F = force exerted by the fluidizing medium on the particles in the bed [N]

G = effective weight of material in the bed [N]

H = height of the fluidized bed [m]

H_T = overall height of the tapered-bed section [m]

h_0 = $\frac{\ell_0}{2\tan\frac{\Theta}{2}}$, the distance between the apex and the bottom of the tapered bed

L = top length of the tapered bed [m]

ℓ = length of the tapered bed [m]

ℓ_0 = length of the bottom of the tapered fluidized bed [m]

ℓ_1 = length of the top of the tapered fluidized bed [m]

$(-\Delta P)$ = pressure drop [N/m^2]

$(-\Delta P_{mf})$ = pressure drop at the minimum fluidizing velocity in a columnar bed [N/m^2]

$(-\Delta P_{max})$ = maximum pressure drop [N/m^2]

u = superficial fluid velocity [m/s]

u_0 = superficial fluid velocity at the bottom of the bed [m/s]

u_c = critical fluidizing velocity in terms of the superficial velocity at the bottom of the fluidized bed [m/s]

u_{mf} = minimum fluidizing velocity in terms of the superficial velocity at the bottom of the fluidized bed

w_0 = width of the tapered bed [m]

ε_0 = void fraction of the packed bed [-]

μ = fluid viscosity [Ns/m^2]

ρ_f = fluid density [kg/m^3]

ρ_s = solid density [kg/m^3]

ϕ_s = sphericity of the solid particles [-]

$Ar = \left(\frac{d_p^3 \rho_f^2 g}{\mu^2} \cdot \frac{\rho_s - \rho_f}{\rho_f}\right)$, Archimedes number [-]

$Eu = \left[\frac{(-\Delta P)}{\rho_f u_0^2}\right]$, Euler number [-]

$Eu_c = \left[\frac{(-\Delta P_{max})}{\rho_f u_c^2}\right]$, Euler number at the maximum pressure drop or critical fluidizing velocity [-]

$Re = \left(\frac{d_p \rho_f u_0}{\mu}\right)$, Reynolds number [-]

$Re_c = \left(\frac{d_p \rho_f u_c}{\mu}\right)$, Reynolds number at the critical fluidizing velocity [-]

REFERENCES

Dighe, S. V.; Blinn, M. B.; Buggy, J. J.; Krasicki, B. R.; Pierce, B. L., Proceedings of the 16th Intersociety Energy Conversion Engineering Conference, ASME, New York, 1981, pp. 1059-1067.

Ergun, S., Chem. Eng. Progr., 1952, 48, 89.

Gelperin, N. I.; Einstein, E. N.; Gelperin, E. N.; Lvova, S. D., Khim. i Tekhn. Topl. i Masel, 1960, 5 (8), 51.

Golubkovich, A. V., Khim. i Neft. Mash., 1975, No. 3, 21.

Ishii, T., Chem. Eng. Sci., 1973, 28, 1121.

Kunii, D.; Levenspiel, O., "Fluidization Engineering" John Wiley & Sons, Inc., New York, 1969.

Levey, R. P. Jr.; De La Garza, A.; Jacobs, S. C.; Heidt, H. M.; Trent, P. E., Chem. Eng. Progr., 1960, 56, 43.

Nishi, Y., Kagaku Kogaku Ronbunshu, 1979, 5, 202.

Pitt, W. W.; Hancher, C. W.; Patton, B. D., Nuclear and Chemical Waste Management, 1981, 2, 57.

Ridgway, K., Chem. and Proc. Eng., June, 1965, p. 317.

Scott, C. D.; Hancher, C. W., Biotechnology and Bioengineering, 1976, 18, 1393-1403.

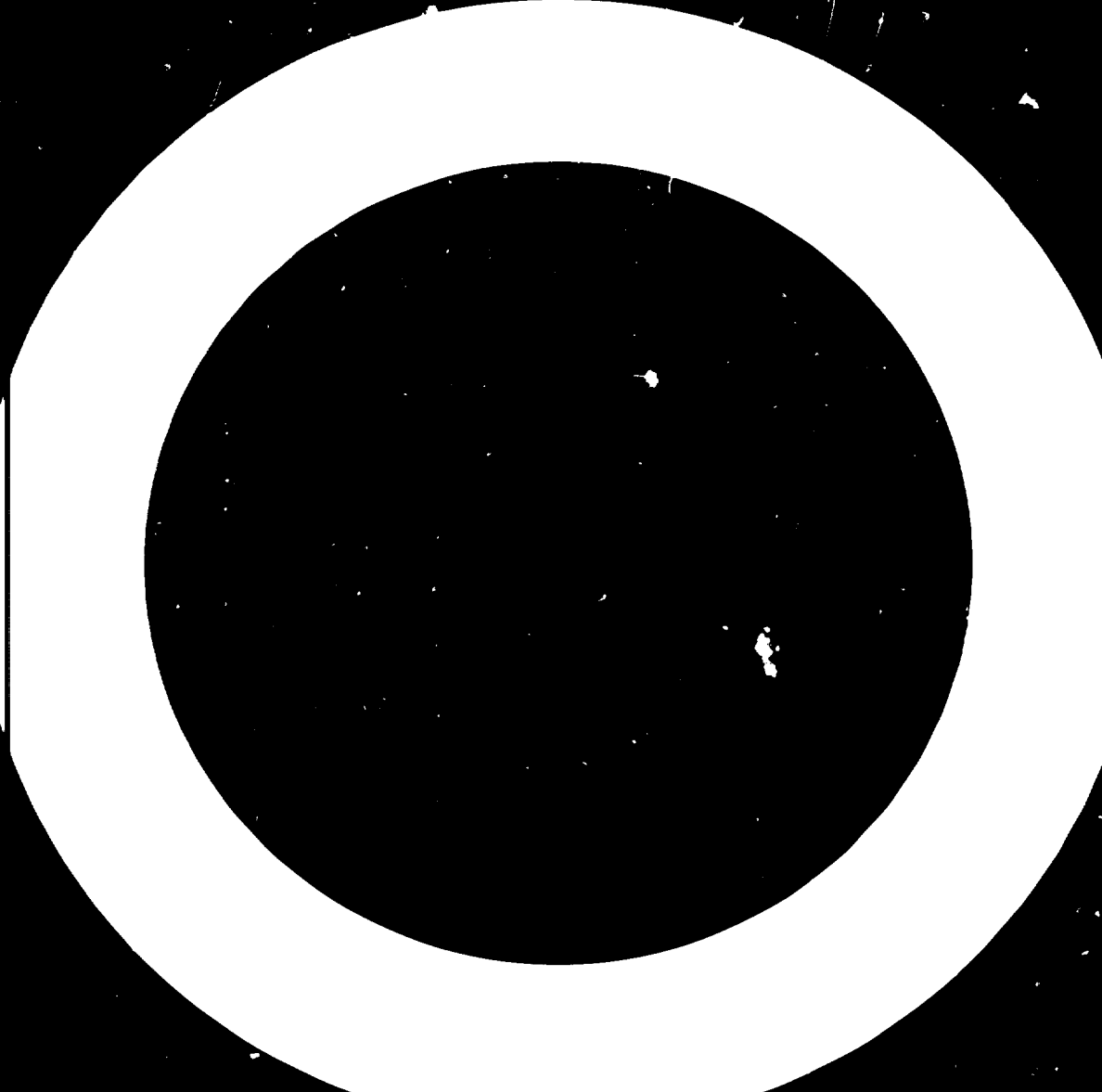

Table 2. Properties of solid particles.

Material	d_p [mm]	ρ_s [kg/m^3]	ε_{mf} [-]
Silica gel	1.125	2590	0.346
Sand	0.711	2590	0.386

List of Figure Captions

Fig. 1. Pressure drop-velocity relations for the columnar and tapered fluidized beds with the same initial packed height.

Fig. 2. Structure of the tapered fluidized bed.

Fig. 3. Schematic of the experimental set-up.

Fig. 4. Comparison of the pressure drop through the tapered packed bed computed by equation (5a) or (5b) with the experimental data.

Fig. 5. Comparison between the experimentally measured critical fluidizing velocity, $(u_c)_{exp}$, and the calculated fluidizing velocity, $(u_c)_{cal}$.

Fig. 6. Comparison between the experimentally measured maximum pressure drop, $(-\Delta P_{max})_{exp}$, and the calculated maximum pressure drop, $(-\Delta P_{max})_{cal}$.

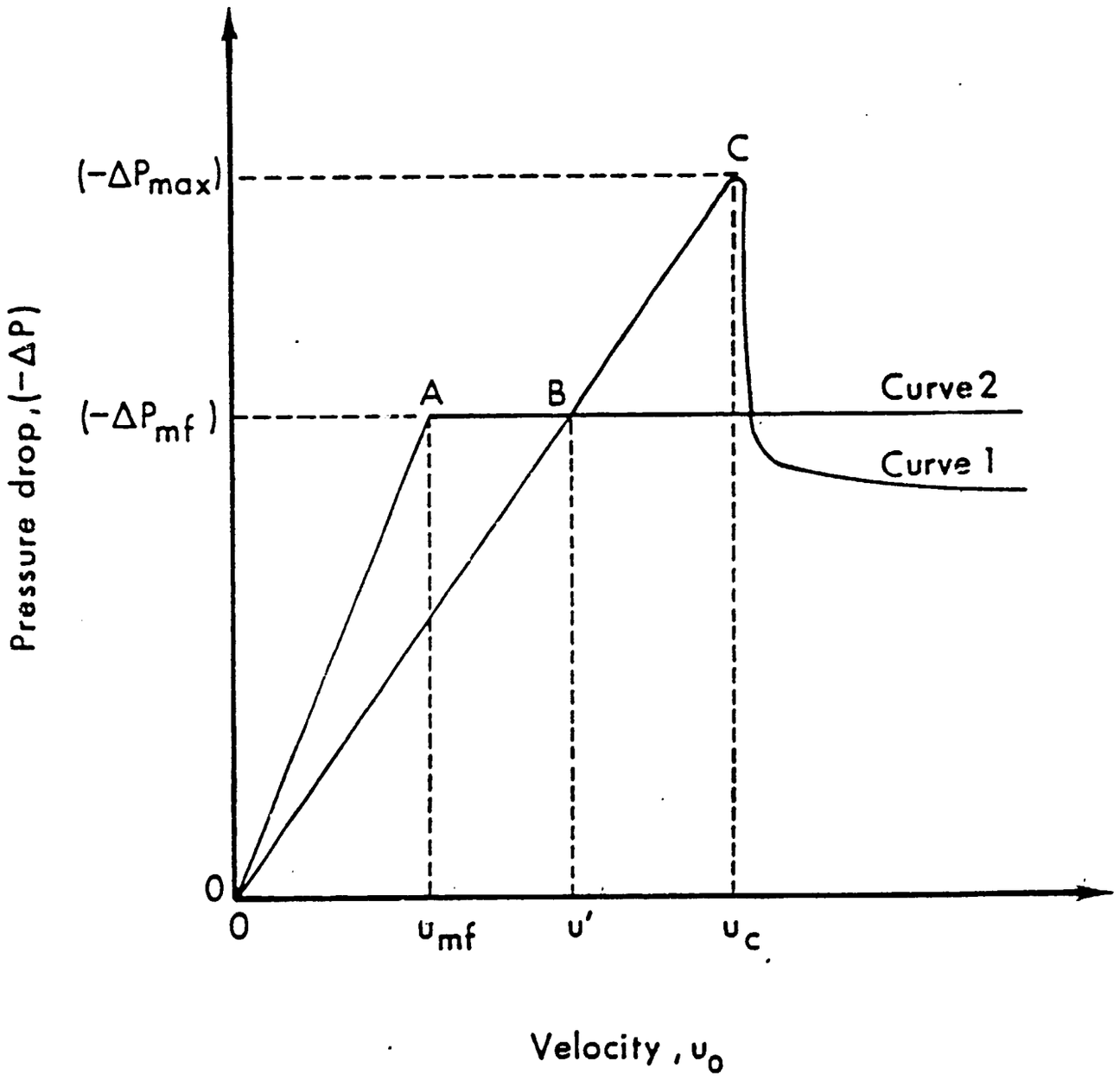

Fig 1 Pressure drop-velocity relations for the columnar and tapered fluidized beds with the same initial packed heigh

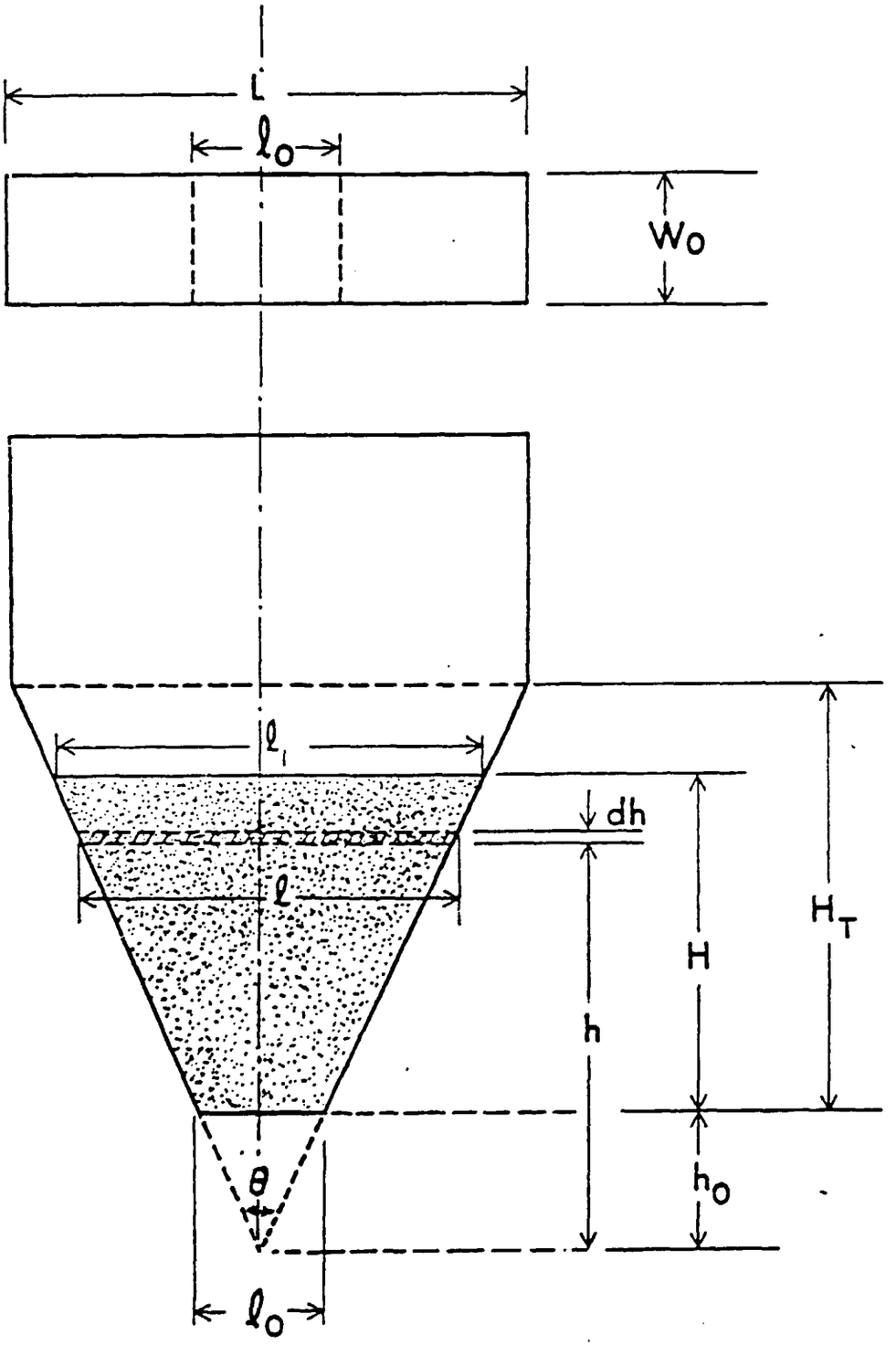

Fig. 2. Structure of the tapered fluidized bed.

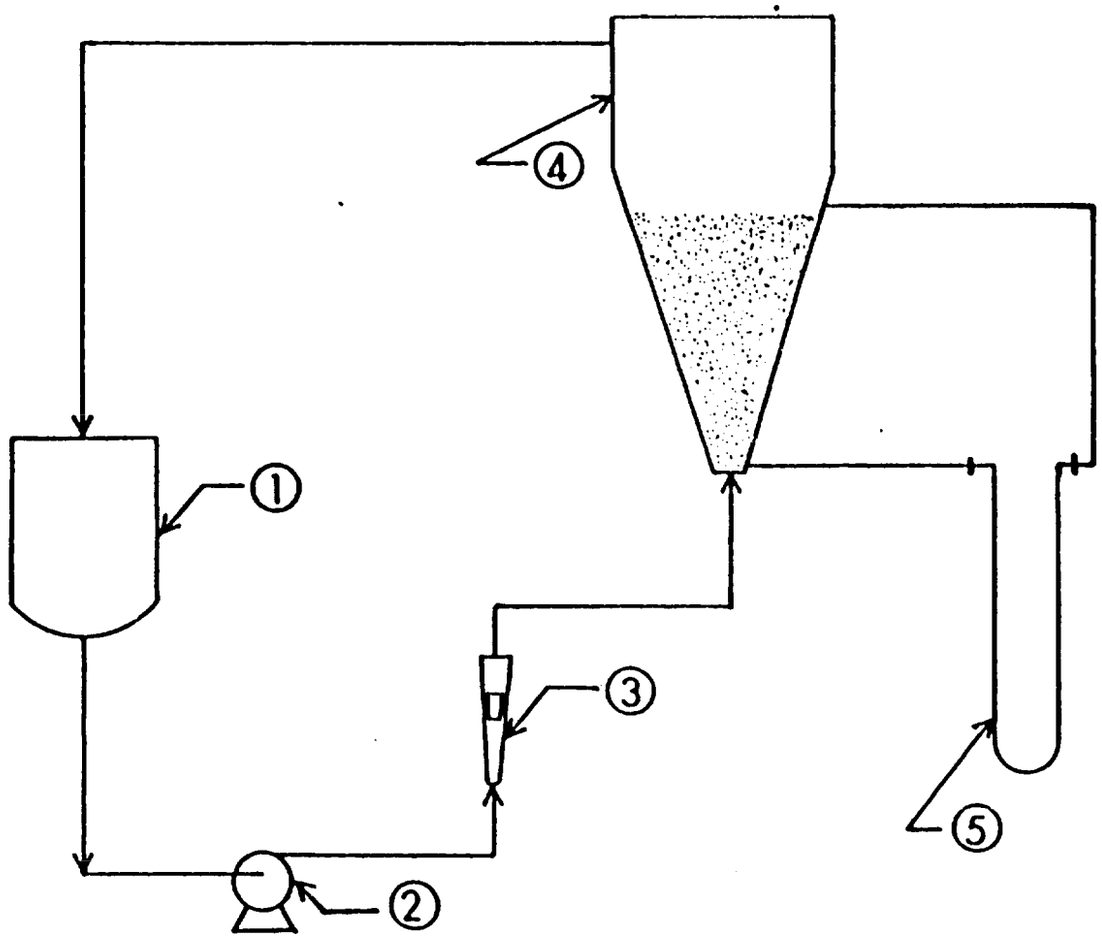

① : Water storage tank
② : Pump
③ : Rotameter
④ : Tapered fluidized bed
⑤ : Piezometer

Fig.3. Schematic of the experimental set-up.

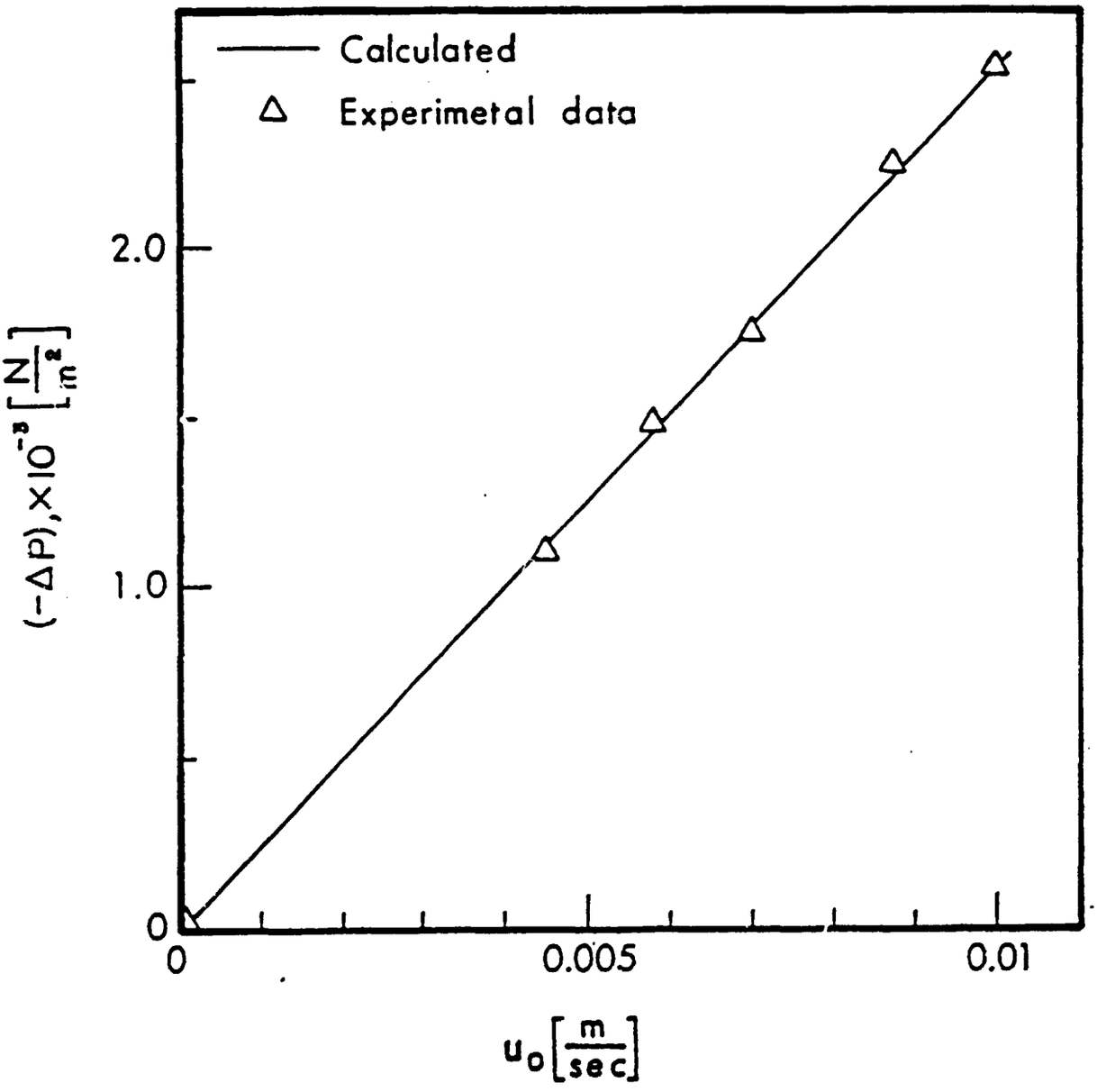

Fig. 4. Comparison of the pressure drop through the tapered packed bed computed by equation (5a) or (5b) with the experimental data.

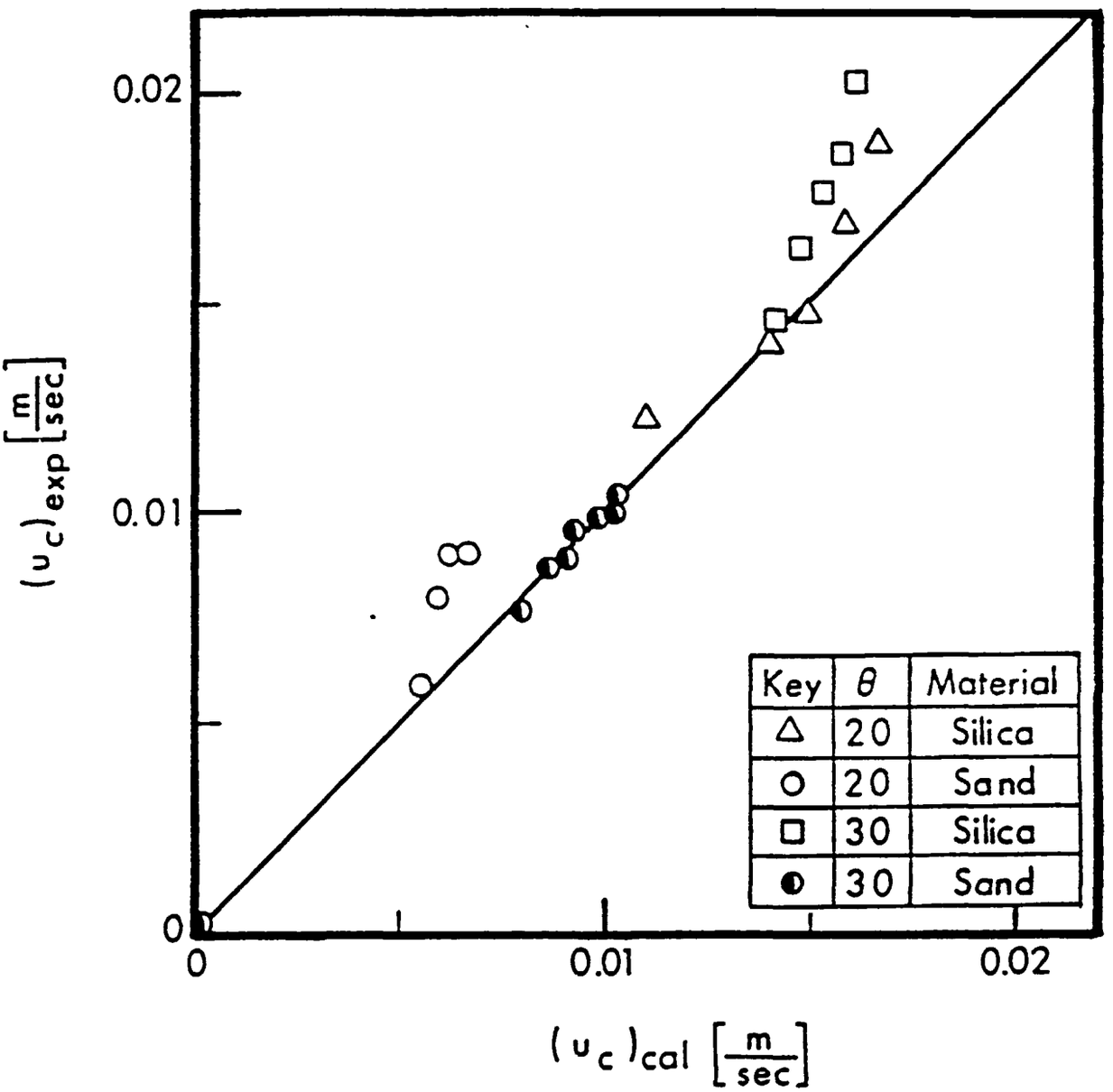

Fig. 5. Comparison between the experimentally measured critical fluidizing velocity, $(u_c)_{exp}$, and the calculated critical fluidizing velocity, $(u_c)_{cal}$.

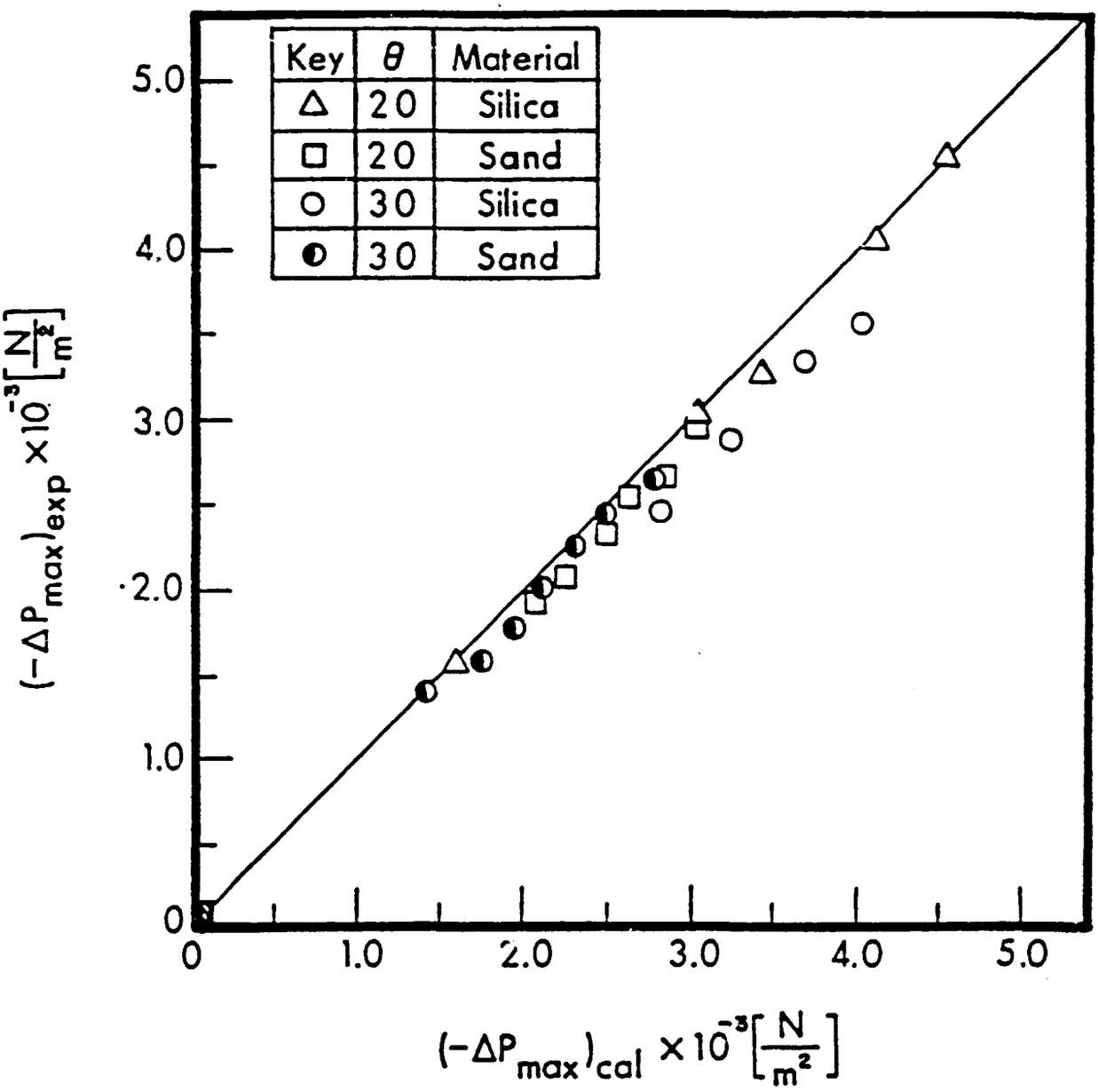

Fig. 6. Comparison between the experimentally measured maximum pressure drop, $(-\Delta P_{max})_{exp}$, and the calculated maximum pressure drop, $(-\Delta P_{max})_{cal}$.